nanomaterials

MDPI

Article

Sodium-Based Cylindrical Plasmonic Waveguides in the Near-Infrared

Da Teng [1,*], Yuanming Tian [1], Xuemei Hu [1], Ziyi Guan [1], Wencang Gao [1], Pengyuan Li [1], Hongli Fang [1], Jianjun Yan [1], Zhiwen Wang [1] and Kai Wang [2,*]

[1] College of Physics and Electronic Engineering, Zhengzhou Normal University, Zhengzhou 450044, China; tianyuanming_8426@163.com (Y.T.); hu19139279202@163.com (X.H.); guanziyi0505@163.com (Z.G.); gwc315760@163.com (W.G.); m13213001330@163.com (P.L.); fhl_liquid@163.com (H.F.); yjj_llxl@163.com (J.Y.); zwwang@zznu.edu.cn (Z.W.)

[2] Key Laboratory of Infrared Imaging Materials and Detectors, Shanghai Institute of Technical Physics, Chinese Academy of Sciences, Shanghai 200083, China

* Correspondence: tengda@zznu.edu.cn (D.T.); wangkai@mail.sitp.ac.cn (K.W.)

Abstract: Subwavelength optical field confinement and low-loss propagation are of great significance for compact photonic integration. However, the field confinement capability of plasmonic devices is always accompanied by the inherent Ohmic loss. Although recent studies have shown that sodium (Na) exhibits lower loss than noble metals in the near-infrared band, the field confinement ability has not been adequately assessed. Meanwhile, the high chemical reactivity of Na should be regulated for practical application. Two dielectric-coated Na nanowires, consisting of cylindrical Na nanowires with one or two dielectric layers as claddings, are proposed and investigated in this paper. Based on finite element calculations, we thoroughly study the modal fields and low-loss propagation properties of dielectric-coated Na nanowires. The results demonstrate that Na exhibits lower loss and stronger field confinement than the typical plasmonic material silver. These findings indicate the performance of plasmonic devices can be considerably improved by employing the metal Na compared with devices using noble metals, which may promote the applications in subwavelength photonic devices.

Keywords: plasmonic waveguide; field confinement; near-infrared; quality factor

Citation: Teng, D.; Tian, Y.; Hu, X.; Guan, Z.; Gao, W.; Li, P.; Fang, H.; Yan, J.; Wang, Z.; Wang, K. Sodium-Based Cylindrical Plasmonic Waveguides in the Near-Infrared. *Nanomaterials* **2022**, *12*, 1950. https://doi.org/10.3390/nano12121950

Academic Editor: José Antonio Sánchez-Gil

Received: 4 May 2022
Accepted: 6 June 2022
Published: 7 June 2022

1. Introduction

Surface plasmons (SPs) [1] have been considered as prospective candidates for the integration and miniaturization of photonic components and circuits, owing to their remarkable capabilities of squeezing light into regions far smaller than the diffraction limit [2,3]. Various noble metal-based designs have been suggested and investigated to support well-confined SP modes, including nanowires [4–8], slot waveguide [9–11], dielectric-loaded waveguide [12], long-range waveguide [13], and wedge waveguide [14], to mention a few. Due to the presence of metal (usually gold and silver), SP waveguides inevitably suffer from high propagation loss, and there exist trade-offs between losses and confinements for plasmonic waveguides stated above. These structures have either poor field confinement or high loss, hindering their applications where both subwavelength confinement and long-range propagation are needed.

To alleviate this conflict, hybrid plasmonic waveguides (HPWs) [15–28] have been proposed and demonstrated, which combine the benefits of both low-loss properties of dielectric fibers and strong field confinement of plasmonic waveguides. However, for practical applications, the loss of these structures is still unacceptably high. Thus, searching for better plasmonic materials [29–31] has become a hot topic. In recent years, researchers have suggested some available materials for supporting SPs, such as nitrides [31], transparent conducting oxide [32], graphene [33–41], transition metal dichalcogenides [42–44], bulk Dirac semimetals [45–47], borophene [48–50], etc. Although some of these materials

support SP modes with strong field confinement and even tunable characteristics, the loss is still unsatisfactory, making them less suitable for real-life applications.

Quite recently, researchers reported [51] a plasmonic nanolaser based on alkali metal Na, which has a lasing threshold lower than previously reported at near-infrared wavelengths. In this work, researchers developed a thermo-assisted spin-coating process for fabricating a high-quality Na film and experimentally measured the dielectric function of Na in the wavelength range 400–1500 nm using a spectroscopic ellipsometer. Notably, the optical damping rate of Na is only half of that of silver. Hence, Na seems to be an ideal plasmonic material with much lower loss than gold and silver from ultraviolet to the near-infrared band. Then, research on propagating and localized Na plasmons was carried out. Tao et al. [52,53] proposed and studied directional couplers based on Na plasmonic waveguide. Abdelsalam et al. [54] investigated localized electromagnetic modes of Na nanoparticles. Recently, SPs were excited at the interface of sodium and graphene [55].

For plasmonic waveguides, both low-loss propagation and strong optical field confinement are of great importance. To our knowledge, although reports have shown that Na exhibits lower loss than gold and silver in the near-infrared band, the field confinement ability has not been properly assessed. Meanwhile, the high chemical reactivity of Na [51] should be controlled for practical application. Here, we propose and investigate two dielectric-coated Na nanowires, consisting of a cylindrical Na nanowire and one or two dielectric layers as claddings. We first compare the permittivity and quality factor of metal Na and Ag, then systematically study the modal field confinement ability and low-loss propagation properties. Meanwhile, we compare the subwavelength propagation properties of dielectric-coated Na and Ag nanowires. The findings reveal that Na nanowires exhibit not only lower loss, but also stronger field confinement than the typical plasmonic material silver, which makes it quite suitable to serve as building blocks for subwavelength photonic devices.

2. Theory

To quantitatively analyze the loss of Na- and Ag-based plasmonic waveguides, we need to obtain the dielectric permittivity. The permittivity of Ag (ε_{Ag}) is adopted from Yang's experimental data [56], while for Na, we use a Drude–Lorentz model to calculate the dielectric permittivity (ε_{Na}), which is expressed as [51]:

$$\varepsilon_{Na}(\omega) = \varepsilon_1 + i\varepsilon_2 = \varepsilon_b - \frac{\omega_p^2}{\omega^2 + i\omega\gamma_p} + \frac{f_1\omega_1^2}{\omega_1^2 - \omega^2 - i\omega\gamma_1} \quad (1)$$

where $\varepsilon_b = 0.5$, $\omega_p = 5.414$ eV, $\gamma_p = 0.01$ eV, $f_1 = 0.28$, $\omega_1 = 2.945$ eV, and $\gamma_1 = 2.706$ eV.

The permittivity and quality factor ($-\varepsilon_1/\varepsilon_2$) of metal Na and Ag are compared in Figure 1 across the wavelength range of 800 to 1500 nm. As seen in Figure 1a, the absolute value of Re(ε_{Ag}) is larger than that of Na, while Im(ε_{Na}) (related to loss) is smaller than that of Ag, and the discrepancy grows as the wavelength increases. Thus, we conclude that the loss of Na is lower than that of Ag, especially at longer wavelengths. In Figure 1b, we see the quality factor of Na firstly increases with the increase in wavelength. When the wavelength exceeds 1200 nm, the quality factor of Na approaches its maximum value and then has a slight downward trend, while the quality factor of Ag monotonically decreases when λ ranges from 800 to 1500 nm.

Considering the fundamental plasmon mode (TM_0) propagating in the z-direction with a complex propagation constant $\beta = n_{eff}k_0$, $k_0 = 2\pi/\lambda$, with λ being the wavelength in vacuum, and $n_{eff} = n_{eff\_r} + in_{eff\_i}$ is the complex effective mode index. Propagation length is defined by $L_P = 1/k_0 n_{eff\_i}$ and normalized mode area is defined by $A_N = A_{eff}/A_0 = \iint W(r)d^2r/\max\{W(r)\}/(\lambda^2/4)$, where $W(r)$ is the energy density of the plasmon mode [15]. Figure of merit (FoM) [57] is given by $L_P/(A_{eff}/\pi)^{1/2}$. The results are obtained by use of the wave optics module of COMSOL Multiphysics, which is widely used for simulating plasmonic devices [58–61]. The eigenvalue solver is used to find modes

of the waveguide. The calculation domain has a radius of 5λ, and a perfectly matched layer (PML) is applied at the outer boundary to keep away from the influence of reflection. A convergence analysis is also conducted to ensure that the numerical boundaries and meshing sizes do not interfere with the solutions.

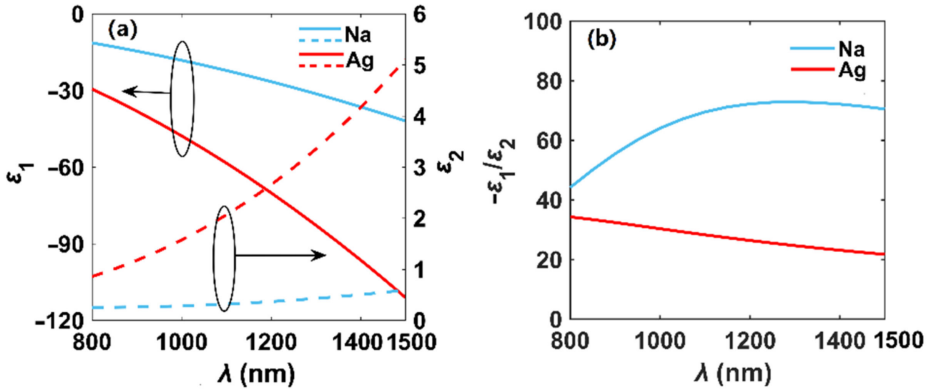

Figure 1. Permittivity ($\varepsilon = \varepsilon_1 + i\varepsilon_2$) (**a**) and quality factor ($-\varepsilon_1/\varepsilon_2$) (**b**) of Na and Ag. The solid and dashed lines of (**a**) stand for the real and imaginary parts of the permittivity, respectively.

3. Results and Discussion

3.1. Modal Properties in Dielectric-Coated Metallic Nanowires (DCMNW)

Figure 2 depicts the schematic of DCMNWs, where r is the radius of the nanowire, and t is the thickness of the dielectric layer with permittivity of $\varepsilon_{SiO2} = 2.25$ [62]. The whole structure is located in vacuum with $\varepsilon_0 = 1$. We first investigate the modal field distributions in DCMNWs by setting $\lambda = 1300$ nm, $r = 100$ nm, and $t = 0$, 20, 80 nm. The special case of $t = 0$ nm corresponds to a single metallic nanowire in vacuum. The 2D modal field distributions of dielectric-coated Na and Ag nanowires are shown in Figure 3a,b, respectively. Clearly, the fundamental plasmon mode (TM_0 with field components of E_r, H_φ, E_z) has a radially polarized electric field, which exponentially decays away from the metal surface. To obtain an intuitive observation, we plot the fields along the x-direction in Figure 3c. The field penetrates through the dielectric-coated Na nanowire, while the fields inside dielectric-coated Ag nanowires have zero value points. Furthermore, compared with that of Na, the field confinement is even weaker for the dielectric-coated Ag nanowire. For instance, the full width at half maximums (FWHMs) of the field plots corresponding to $t = 0$, 20, and 80 nm are 378, 432, and 570 nm for Ag, while 362, 416, and 509 nm for Na. More importantly, by increasing t, the field diffusion could be suppressed; that is, the field values ($|x| > 600$ nm) decrease as t increases, as shown in the inset of Figure 3c. Figure 3d compares the field distributions along the x-direction for dielectric-coated Na and Ag nanowires with $\lambda = 1300$ and 1500 nm, $t = 20$ nm, and $r = 100$ nm. As the wavelength increases, FWHMs of the field plots slightly enlarge. For $\lambda = 1500$ (1300) nm, FWHMs are 444 (432) nm for Ag and 428 (416) nm for Na. Thus, we can reasonably deduce that (i) the field confinement ability of dielectric-coated Na nanowires is stronger than that of dielectric-coated Ag nanowires (see Figures 4c, 5c and 6c); (ii) increasing the cladding thickness t results in a more restricted modal field (see Figure 6c).

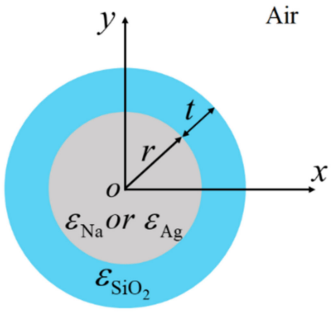

Figure 2. The cross-section of dielectric-coated Ag or Na nanowire.

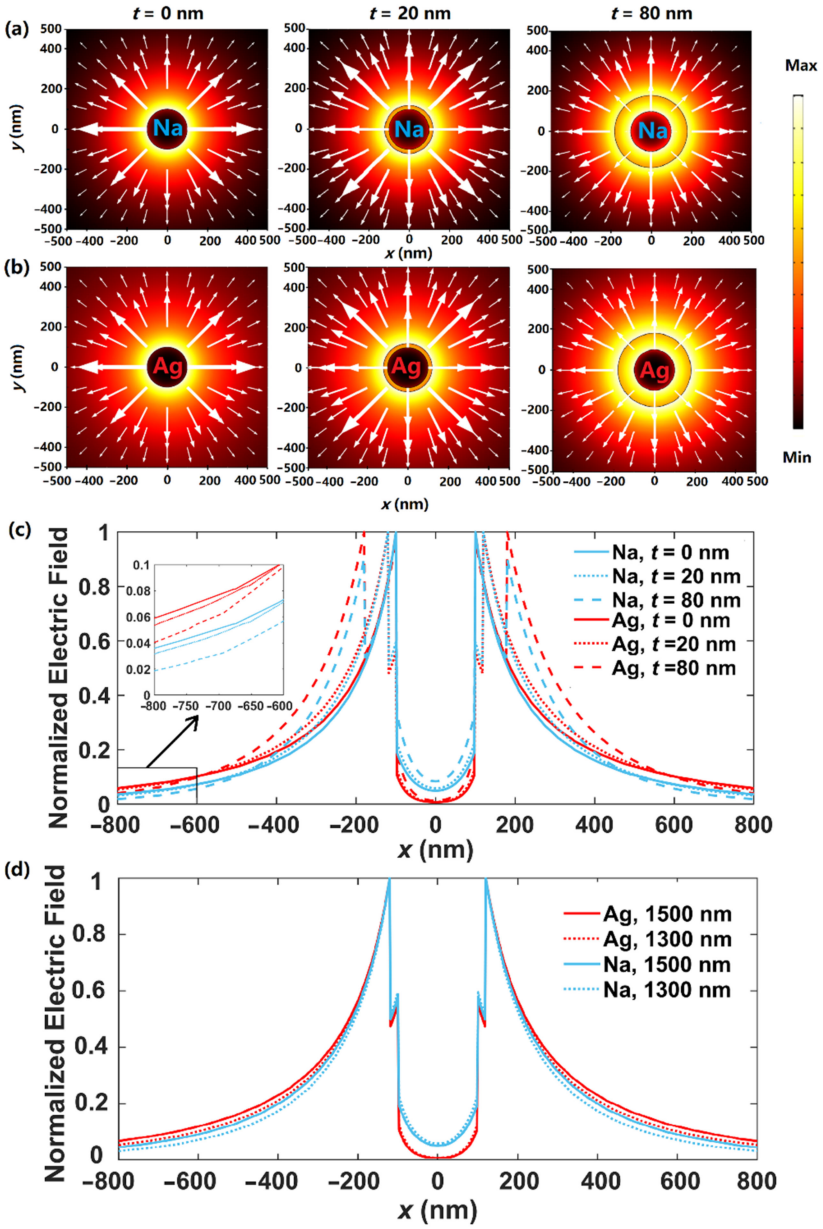

Figure 3. Field distributions of |**E**| of the fundamental mode at λ = 1300 nm for dielectric-coated (**a**) Na and (**b**) Ag nanowires at t = 0, 20, 80 nm. White arrows indicate radially polarized electric fields. (**c**) Field distributions along x-direction. (**d**) Comparison of field distributions along x-direction for λ = 1300 and 1500 nm with t = 20 nm.

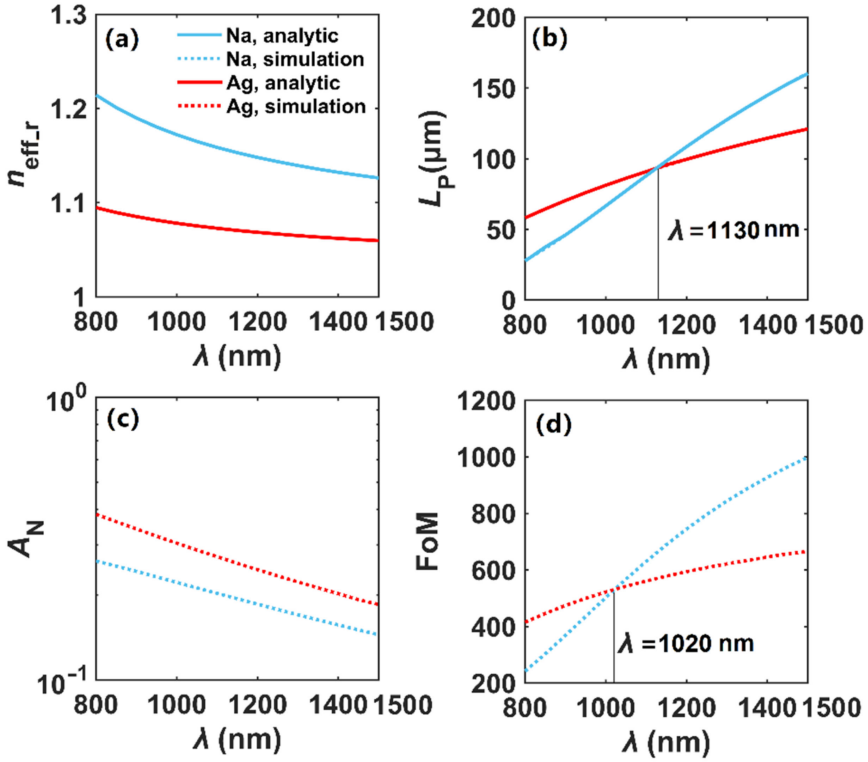

Figure 4. Modal properties of single Na and Ag nanowires in vacuum. (**a**) n_{eff_r}, (**b**) L_P, (**c**) A_N, (**d**) FoM. Analytical results of n_{eff} are obtained from Equation (2) of Ref. [4].

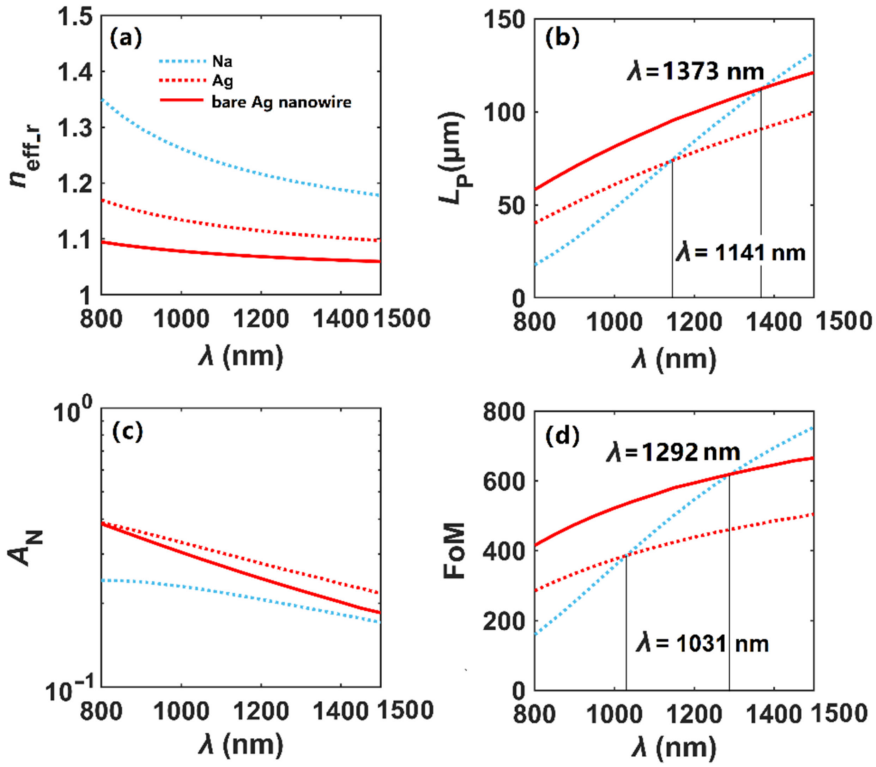

Figure 5. Modal properties of SiO_2-coated Na and Ag nanowires. (**a**) n_{eff_r}, (**b**) L_P, (**c**) A_N, (**d**) FoM.

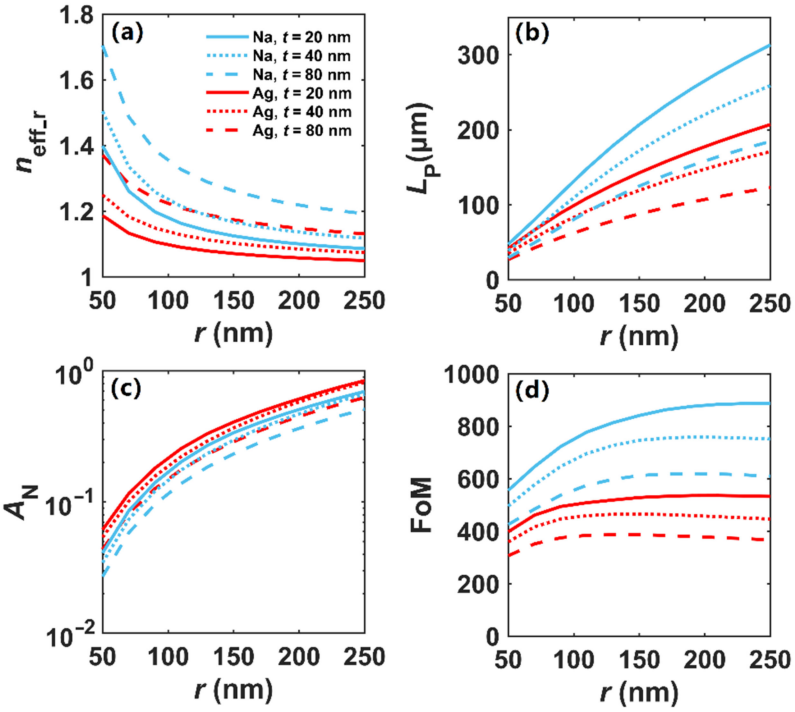

Figure 6. Modal properties of SiO_2-coated Na and Ag nanowires with different radii. (**a**) n_{eff_r}, (**b**) L_P, (**c**) A_N, (**d**) FoM.

In Figure 4, we evaluate the transmission characteristics of Na and Ag nanowires and perform the benchmark work by comparing the analytical results of n_{eff} [4] and the simulated ones, where r = 100 nm and t = 0 nm. As shown in Figure 4a, we can see the n_{eff_r} of the plasmon modes in Na and Ag nanowires decrease with increasing wavelength, and the solid lines and dot lines are highly overlapped, indicating that the simulated and analytical results are in good agreement. The propagation lengths increase for both Na and Ag nanowires, as shown in Figure 4b. However, when λ exceeds 1130 nm, the L_P of the mode in the Na nanowire is larger than that of the Ag nanowire. Meanwhile, as shown in Figure 4c, the modal field area of the fundamental plasmon mode in the Na nanowire is always smaller than Ag throughout the whole wavelength range, implying that the Na nanowire has stronger field confinement ability than the Ag nanowire. Finally, in Figure 4d, we can see that the FoM increases, and when λ exceeds 1020 nm, the FoM of Na-based plasmon mode is much larger. Therefore, the plasmonic effect of Na is better than Ag at longer wavelengths, which is consistent with the results described in Figure 1.

In Figure 5, we study the transmission characteristics of Na and Ag nanowires (r = 100 nm) coated with a silica layer of t = 20 nm at different wavelengths. A bare Ag nanowire is also investigated for comparison. As shown in Figure 5a, the n_{eff_r} of the plasmon modes in Na and Ag nanowires decreases with the increase in λ, while L_P increases with the increase in λ shown in Figure 5b. When λ exceeds 1141 nm, the L_P of the mode in the silica-coated Na nanowire is larger than that of the silica-coated Ag nanowire. When λ exceeds 1373 nm, the L_P of the mode in the silica-coated Na nanowire is even larger than that of a bare Ag nanowire. As in Figure 4c, it can be seen from Figure 5c that the modal field area of the fundamental plasmon mode in the silica-coated Na nanowire is smaller than both silica-coated and bare Ag nanowires throughout the entire wavelength range, indicating that the dielectric-coated Na nanowire has stronger field confinement ability than dielectric-coated and bare Ag nanowires. Finally, we can see from Figure 5d that the FoM increases, and when λ exceeds 1292 nm, the FoM of the Na-based plasmon mode is much larger. As seen in Figure 5b,c, the silica-coated Na nanowire outperforms its silver counterpart in both field confinement and propagation loss when λ > 1141 nm, and

the silica-coated Na nanowire also outperforms the bare silver nanowire when $\lambda > 1373$ nm. As a result, λ is set to be 1500 nm in the following.

Then, with r varying from 50 to 250 nm, we investigate the modal transmission characteristics of Na and Ag nanowires coated with various thicknesses of silica, where λ = 1500 nm and t = 20, 40, and 80 nm. In Figure 6a, we observe that the $n_{\text{eff\_r}}$ of the plasmon modes in dielectric-coated Na and Ag nanowires decrease with the increase in nanowire radius, and $n_{\text{eff\_r}}$ of Na plasmon modes are larger than those of Ag under the same thickness of silica. When $r > 200$ nm, the effective mode index $n_{\text{eff\_r}}$ tends to be stable and decreases slowly. As shown in Figure 6b, the modal propagation lengths in both silica-coated Na and Ag nanowires increase with the increase in r, and Na nanowires have an advantage over Ag nanowires in the propagation distance with the same value of t. For instance, the L_P of silica-coated Na and Ag is about 313 μm (i.e., 208.6λ) and 207 μm (i.e., 138λ) when r = 250 nm and t = 20 nm, respectively. Meanwhile, as seen in Figure 6c, the modal field area of silica-coated Na nanowires is smaller than that of Ag when the thicknesses of SiO_2 are set to be the same. By increasing the cladding thickness t, a more confined modal field could be achieved. Apparently, the trade-off between loss and field confinement still exists. When enlarging r, the field confinement weakens, while the propagation length increases. As shown in Figure 6d, the FoM of silica-coated Na could reach as high as 886, while that of silica-coated Ag is only 533 when r = 250 nm and t = 20 nm, and the FoM tends to be stable when r exceeds 150 nm.

3.2. Modal Properties in Double Dielectric-Coated Metallic Nanowires (DDCMNWs)

By adding another high-index dielectric layer to the DCMNWs, one can easily form the double dielectric-coated metallic nanowires (DDCMNWs), as shown in Figure 7. t_h is the thickness of the high-index dielectric layer with permittivity of ε_{Si} = 12.25 [63]. The modal field distributions in DDCMNWs are investigated by setting λ = 1500 nm, r = 100 nm, t = 2, 10 nm, and t_h = 200 nm. The 2D modal field distributions of DDCMNWs based on Na and Ag are depicted in Figure 8a,b, respectively. Clearly, the optical energy is mainly concentrated inside the gap region between the metal nanowire and outside the high-index dielectric layer. As shown in Figure 8c, the field distributions inside the nanowires are similar to those shown in Figure 3c; that is, the fields penetrate through the Na nanowires, while the fields inside Ag nanowires have zero value points. Moreover, at the outside boundaries of the high-index materials, the field values of dielectric-coated Ag nanowires are larger than those of Na nanowires, which indicates the field confinement of the Ag-based DDCMNW is weaker compared with that of the Na-based DDCMNW.

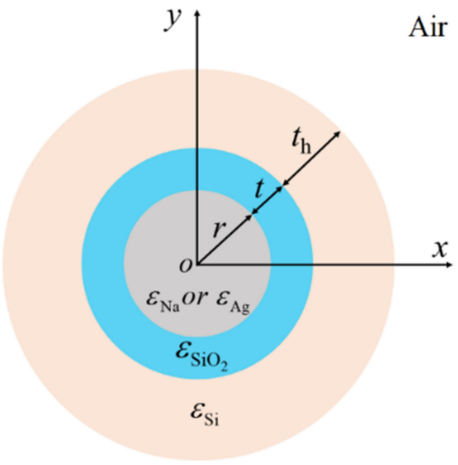

Figure 7. The cross-section of DDCMNWs based on Ag or Na nanowires.

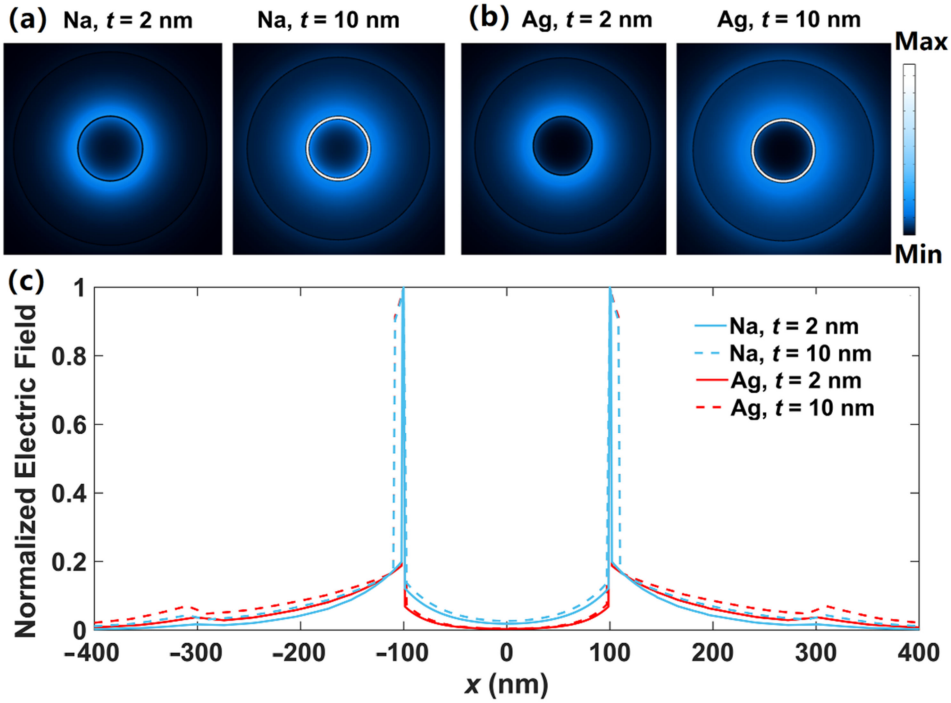

Figure 8. Field distributions of |**E**| of the fundamental mode in DDCMNWs at λ = 1500 nm for (**a**) Na and (**b**) Ag. (**c**) Field distributions along x-direction.

In Figure 9, we study the modal properties of DDCMNWs based on Na and Ag nanowires with different cladding thicknesses t_h. As shown in Figure 9a,b, the n_{eff_r} of the plasmon modes in Na and Ag DDCMNWs firstly increases with the increment of cladding thickness t_h and then tends to be invariable when t_h > 150 nm, while the propagation length increases with the increment of t_h. For a smaller gap distance, i.e., t = 2 and 5 nm, L_P tends to be stable when t_h > 300 nm. It is worth to be noted that when for t_h > 365 nm and t = 10 nm, the loss of the Ag-based DDCMNW becomes smaller than that of Na, whereas, the plasmon modal field area of the Na-based DDCMNW is smaller than those of Ag throughout the whole t_h range shown in Figure 9c. This indicates that the field confinement of the Na-based DDCMNW is superior to that of the Ag-based DDCMNW. Meanwhile, the smaller the gap distance, the stronger the field confinement. For t_h = 300 nm and t = 2, 10 nm, A_N is 0.0123 and 0.0307 for the Na-based DDCMNW, respectively. Finally, in Figure 9d, we can see that the FoM increases for both Na- and Ag-based DDCMNWs. The Na-based DDCMNW has a larger FoM than Ag for the same t. Therefore, the results show that the plasmonic effect of Na is better than that of Ag; that is, Na-based plasmons exhibit not only lower loss, but also stronger field confinement than the typical plasmonic material Ag when t_h < 365 nm.

Although SiO_2-Si double dielectric-coated metal nanowires (DDCMNWs) exhibit relatively strong dissipation and significantly smaller propagation distances (Figure 9b) than SiO_2 coated metal nanowires (DCMNWs) (Figure 6b), their major advantage is the possibility of stronger subwavelength confinement of the guided modes (smaller A_N, see Figures 6c and 9c), which is one of the major requirements for interconnects in highly integrated optical circuits and subwavelength optical devices.

Finally, we need to explain here that we only consider the comparison between Na and Ag for reasons listed below. Different metals have been employed to excite SPs in different frequency bands in the literature. For instance, copper is used in the terahertz band [64]. Aluminum (Al) possesses material properties that enable strong plasmon resonances spanning much of the visible region and into the ultraviolet [65], while silver and gold are often used in the visible region and near infrared [29]. In terms of SP waveguiding, silver provides a larger FoM than gold (see Figures 18 and 19 of Ref. [30]). As a result, we

skip the comparison between Na and Au and conclude that Na-based plasmon modes outperform Ag- and Au-based plasmon modes in terms of subwavelength waveguiding.

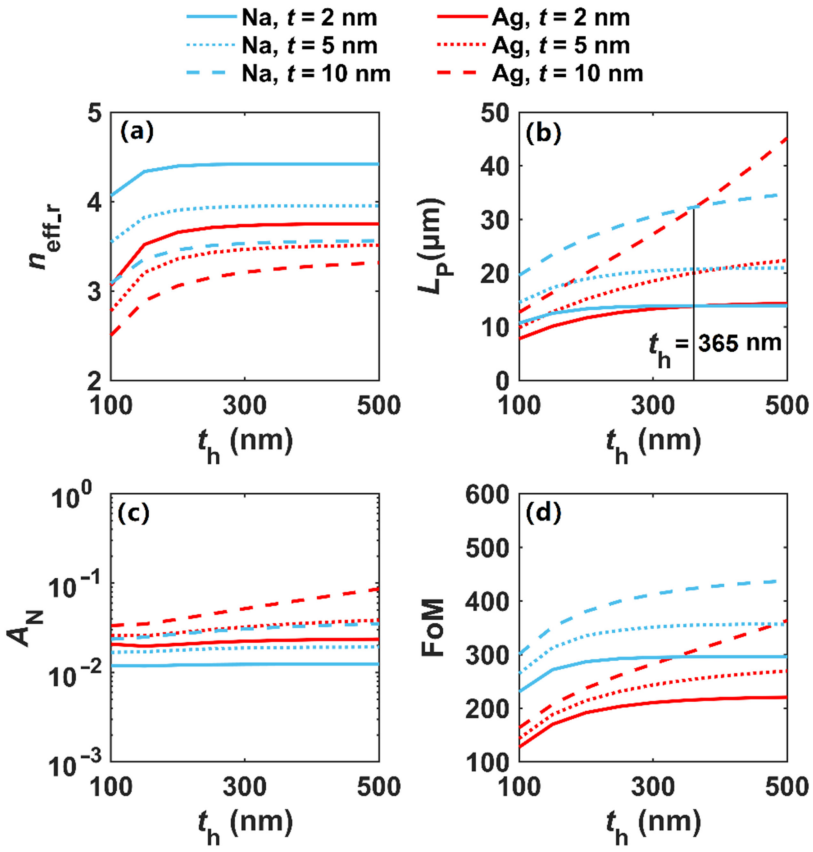

Figure 9. Modal properties of DDCMNWs based on Na and Ag with different cladding thickness t_h at λ = 1500 nm. (**a**) n_{eff_r}, (**b**) L_P, (**c**) A_N, (**d**) FoM. Thicknesses of SiO_2 are set to be t = 2, 5, 10 nm and r = 100 nm.

4. Conclusions

We propose and investigate (double) dielectric-coated Na nanowires by using finite element calculations. Increasing the cladding thickness t of the dielectric-coated Na nanowires results in a more confined modal field. The silica-coated Na nanowire outperforms its silver counterpart in terms of field confinement and propagation loss when $\lambda > 1141$ nm and also outperforms the bare silver nanowire when $\lambda > 1373$ nm. The L_P and FoM of the silica-coated Na nanowire are about 208.6λ and 886 when r = 250 nm and t = 20 nm. For double dielectric-coated Na nanowires, the loss and normalized modal field area are both smaller compared with those of Ag-based nanowire waveguides when $t_h < 365$ nm. The obtained results suggest Na-based plasmons exhibit not only lower loss, but also stronger field confinement than the typical plasmonic material Ag at longer wavelengths, which implies the subwavelength waveguiding performance of plasmonic devices can be greatly improved by using Na. These results may have potential applications in the fields of subwavelength photonic devices, such as nanolasers, resonators, sensors, and other waveguide-integrated devices.

Author Contributions: Conceptualization, D.T.; writing—original draft preparation, D.T., Y.T., X.H., Z.G., W.G., P.L. and H.F.; writing—review and editing, Y.T., X.H., Z.G. and Z.W.; visualization, W.G., P.L. and J.Y.; supervision, D.T. and K.W. All authors have read and agreed to the published version of the manuscript.

Funding: This work was supported by the Natural Science Foundation of Shanghai (20ZR1466200, 21ZR1474000), Natural Science Foundation of Henan (222300420378), Key Scientific Research Project of Colleges and Universities in Henan Province (21A140029, 22B140008), Technologies Research and Development Program of Henan Province (212102210486), Young Backbone Teacher Training Program of Zhengzhou Normal University (QNGG-20774), Scientific Research Innovation Foundation for Students of Zhengzhou Normal University (2021003), Open Research Fund of Zhengzhou Normal University, and Scientific Research Starting Foundation of Zhengzhou Normal University.

Institutional Review Board Statement: Not applicable.

Informed Consent Statement: Not applicable.

Data Availability Statement: The data presented in this study are available on request from the corresponding author.

Conflicts of Interest: The authors declare no conflict of interest.

References

1. Achanta, V.G. Surface waves at metal-dielectric interfaces: Material science perspective. *Rev. Phys.* **2020**, *5*, 100041. [CrossRef]
2. Li, S.; Zuo, G.; Wu, N.; Yang, Z.; Zhao, B.; Xia, L.; Li, W. Hybrid plasmonic nanofocusing waveguide for on-chip SERS tweezer. *Opt. Laser Technol.* **2021**, *143*, 107259. [CrossRef]
3. Gramotnev, D.K.; Bozhevolnyi, S.I. Plasmonics beyond the diffraction limit. *Nat. Photon.* **2010**, *4*, 83–91. [CrossRef]
4. Stockman, M.I. Nanofocusing of optical energy in tapered plasmonic waveguides. *Phys. Rev. Lett.* **2004**, *93*, 137404. [CrossRef] [PubMed]
5. Wei, H.; Pan, D.; Zhang, S.; Li, Z.; Li, Q.; Liu, N.; Wang, W.; Xu, H. Plasmon waveguiding in nanowires. *Chem. Rev.* **2018**, *118*, 2882–2926. [CrossRef]
6. Liaw, J.W.; Mao, S.Y.; Luo, J.Y.; Ku, Y.C.; Kuo, M.K. Surface plasmon polaritons of higher-order mode and standing waves in metallic nanowires. *Opt. Express* **2021**, *29*, 18876–18888. [CrossRef]
7. Teng, D.; Cao, Q.; Li, S.; Gao, H. Tapered dual elliptical plasmon waveguides as highly efficient terahertz connectors between approximate plate waveguides and two-wire waveguides. *J. Opt. Soc. Am. A* **2014**, *31*, 268–273. [CrossRef] [PubMed]
8. Liu, D.; Zhao, S.; You, B.; Jhuo, S.; Lu, J.; Chou, S.; Hattori, T. Tuning transmission properties of 3D printed metal rod arrays by breaking the structural symmetry. *Opt. Express* **2021**, *29*, 538–551. [CrossRef]
9. Choo, H.; Kim, M.; Staffaroni, M.; Seok, T.J.; Bokor, J.; Cabrini, S.; Schuck, P.J.; Wu, M.C.; Yablonovitch, E. Nanofocusing in a metal–insulator–metal gap plasmon waveguide with a three-dimensional linear taper. *Nat. Photon.* **2012**, *6*, 838–844. [CrossRef]
10. Yang, L.; Xie, X.; Yang, J.; Xue, M.; Wu, S.; Xiao, S.; Song, F.; Dang, J.; Sun, S.; Zuo, Z.; et al. Strong light–matter interactions between gap plasmons and two-dimensional excitons under ambient conditions in a deterministic way. *Nano Lett.* **2022**, *22*, 2177–2186. [CrossRef] [PubMed]
11. Lin, Y.E.; Hsu, W.H.; Huang, C.C. Highly confined dielectric guiding mode in nanoridges embedded in a conventional slot waveguide. *Opt. Express* **2021**, *29*, 16284–16298. [CrossRef]
12. Han, Z.; Radko, I.P.; Mazurski, N.; Desiatov, B.; Beermann, J.; Albrektsen, O.; Levy, U.; Bozhevolnyi, S.I. On-chip detection of radiation guided by dielectric-loaded plasmonic waveguides. *Nano Lett.* **2015**, *15*, 476–480. [CrossRef] [PubMed]
13. Pierre, B. Long-range surface plasmon polaritons. *Adv. Opt. Photon.* **2009**, *1*, 484–588.
14. Moreno, E.; Rodrigo, S.G.; Bozhevolnyi, S.I.; Martín-Moreno, L.; García-Vidal, F.J. Guiding and focusing of electromagnetic fields with wedge plasmon polaritons. *Phys. Rev. Lett.* **2008**, *100*, 023901. [CrossRef]
15. Oulton, R.F.; Sorger, V.J.; Genov, D.A.; Pile, D.F.P.; Zhang, X. A hybrid plasmonic waveguide for subwavelength confinement and long-range propagation. *Nat. Photon.* **2008**, *2*, 496–500. [CrossRef]
16. Ma, Y.; Li, J.; Cada, M.; Bian, Y.; Han, Z.; Ma, Y.; Iqbal, M.; Pištora, J. Plasmon generation and routing in nanowire-based hybrid plasmonic coupling systems with incorporated nanodisk antennas. *IEEE J. Sel. Top. Quantum Electron.* **2021**, *27*, 1–7. [CrossRef]
17. Bian, Y.; Zheng, Z.; Zhao, X.; Zhu, J.; Zhou, T. Symmetric hybrid surface plasmon polariton waveguides for 3D photonic integration. *Opt. Express* **2009**, *17*, 21320–21325. [CrossRef] [PubMed]
18. Chen, L.; Zhang, T.; Li, X.; Huang, W. Novel hybrid plasmonic waveguide consisting of two identical dielectric nanowires symmetrically placed on each side of a thin metal film. *Opt. Express* **2012**, *20*, 20535–20544. [CrossRef]
19. Teng, D.; Wang, Y.; Xu, T.; Wang, H.; Shao, Q.; Tang, Y. Symmetric graphene dielectric nanowaveguides as ultra-compact photonic structures. *Nanomaterials* **2021**, *11*, 1281. [CrossRef]
20. Teng, D.; Cao, Q.; Gao, H.; Wang, K.; Zhu, M. Three-wave approximation for the modal field inside high-index dielectric rods of hybrid plasmonic waveguides. *J. Mod. Opt.* **2016**, *63*, 1451–1456. [CrossRef]
21. Alam, M.Z.; Aitchison, J.S.; Mojahedi, M. A marriage of convenience: Hybridization of surface plasmon and dielectric waveguide modes. *Laser Photon Rev.* **2014**, *8*, 1863–8899. [CrossRef]
22. Dai, D.; He, S. A silicon-based hybrid plasmonic waveguide with a metal cap for a nano-scale light confinement. *Opt. Express* **2009**, *17*, 16646–16653. [CrossRef]

23. Kumar, S.; Kumar, P.; Ranjan, R. A metal-cap wedge shape hybrid plasmonic waveguide for nano-scale light confinement and long propagation range. *Plasmonics* **2022**, *17*, 95–105. [CrossRef]
24. Zhang, Q.; Pan, J.; Wang, S.; Du, Y.; Wu, J. A triangle hybrid plasmonic waveguide with long propagation length for ultradeep subwavelength confinement. *Crystals* **2022**, *12*, 64. [CrossRef]
25. Huang, C.C.; Chang, R.J.; Huang, C.C. Nanostructured hybrid plasmonic waveguide in a slot structure for high-performance light transmission. *Opt. Express* **2021**, *29*, 29341–29356. [CrossRef]
26. Sun, P.; Xu, P.; Zhu, K.; Zhou, Z. Silicon-based optoelectronics enhanced by hybrid plasmon polaritons: Bridging dielectric photonics and nanoplasmonics. *Photonics* **2021**, *8*, 482. [CrossRef]
27. Sun, M.; Tian, J.; Li, L. Mode properties of a coaxial multi-layer hybrid surface plasmon waveguide. *Phys. Status Solidi B* **2015**, *252*, 1884–1889. [CrossRef]
28. Teng, D.; Cao, Q.; Wang, K. An extension of the generalized nonlocal theory for the mode analysis of plasmonic waveguides at telecommunication frequency. *J. Opt.* **2017**, *19*, 055003. [CrossRef]
29. West, P.; Ishii, S.; Naik, G.; Emani, N.; Shalaev, V.M.; Boltasseva, A. Searching for better plasmonic materials. *Laser Photon. Rev.* **2010**, *4*, 795–808. [CrossRef]
30. Naik, G.V.; Shalaev, V.M.; Boltasseva, A. Alternative plasmonic materials: Beyond gold and silver. *Adv. Mater.* **2013**, *25*, 3264–3294. [CrossRef]
31. Boltasseva, A.; Atwater, H.A. Low-loss plasmonic metamaterials. *Science* **2011**, *331*, 290–291. [CrossRef]
32. Zhao, H.; Wang, Y.; Xue, T.; Su, H.; Zhang, J. Direct evidence of visible surface plasmon excitation in ITO film coated on $LiNbO_3$ slabs. *Opt. Express* **2017**, *25*, 6227–6233. [CrossRef]
33. Kim, J.T.; Choe, J.-H.; Kim, J.-S.; Seo, D.; Kim, Y.D.; Chung, K.H. Graphene-based plasmonic waveguide devices for electronic-photonic integrated circuit. *Opt. Laser Technol.* **2018**, *106*, 76–86. [CrossRef]
34. Vakil, A.; Engheta, N. Transformation optics using graphene. *Science* **2011**, *332*, 1291–1294. [CrossRef]
35. Teng, D.; Wang, K. Theoretical analysis of terahertz dielectric-loaded graphene waveguide. *Nanomaterials* **2021**, *11*, 210. [CrossRef]
36. Grigorenko, N.; Polini, M.; Novoselov, K.S. Graphene plasmonics. *Nat. Photon.* **2012**, *6*, 749–758. [CrossRef]
37. Teng, D.; Wang, K.; Huan, Q.; Chen, W.; Li, Z. High-performance light transmission based on graphene plasmonic waveguides. *J. Mater. Chem. C* **2020**, *8*, 6832–6838. [CrossRef]
38. Teng, D.; Wang, K.; Li, Z.; Zhao, Y. Graphene-coated nanowire dimers for deep subwavelength waveguiding in mid-infrared range. *Opt. Express* **2019**, *27*, 12458–12469. [CrossRef]
39. Wu, F.; Liu, D.; Xiao, S. Bandwidth-tunable near-infrared perfect absorption of graphene in a compound grating waveguide structure supporting quasi-bound states in the continuum. *Opt. Express* **2021**, *29*, 41975–41989. [CrossRef]
40. Teng, D.; Wang, K.; Li, Z. Graphene-coated nanowire waveguides and their applications. *Nanomaterials* **2020**, *10*, 229. [CrossRef]
41. Tu, P.Y.; Huang, C.C. Analysis of hybrid plasmon-phonon-polariton modes in hBN/graphene/hBN stacks for mid-infrared waveguiding. *Opt. Express* **2022**, *30*, 2863–2876. [CrossRef]
42. Zheng, K.; Song, J.; Qu, J. Hybrid low-permittivity slot-rib plasmonic waveguide based on monolayer two dimensional transition metal dichalcogenide with ultra-high energy confinement. *Opt. Express* **2018**, *26*, 15819–15824. [CrossRef] [PubMed]
43. Zhang, J.; Hong, Q.; Zou, J.; Meng, Q.; Qin, S.; Zhu, Z. Ultra-narrowband visible light absorption in a monolayer MoS_2 based resonant nanostructure. *Opt. Express* **2020**, *28*, 27608–27614. [CrossRef]
44. Sun, J.; Li, Y.; Hu, H.; Chen, W.; Zheng, D.; Zhang, S.; Xu, H. Strong plasmon–exciton coupling in transition metal dichalcogenides and plasmonic nanostructures. *Nanoscale* **2021**, *13*, 4408–4419. [CrossRef]
45. Timusk, T.; Carbotte, J.P.; Homes, C.C.; Basov, D.N. Dielectric response and novel electromagnetic modes in three-dimensional Dirac semimetal films. *Phys. Rev. B* **2016**, *93*, 235417.
46. He, X.; Liu, F.; Lin, F.; Shi, W. Tunable 3D Dirac-semimetals supported mid-IR hybrid plasmonic waveguides. *Opt. Lett.* **2021**, *46*, 472–475. [CrossRef]
47. He, X.; Lin, F.; Liu, F.; Shi, W. Tunable terahertz Dirac-semimetal hybrid plasmonic waveguides. *Opt. Mater. Express* **2022**, *12*, 73–84. [CrossRef]
48. Liu, T.; Zhou, C.; Xiao, S. Tailoring anisotropic absorption in a borophene-based structure via critical coupling. *Opt. Express* **2021**, *29*, 8941–8950. [CrossRef]
49. Zhang, J.; Zhang, Z.; Song, X.; Zhang, H.; Yang, J. Infrared plasmonic sensing with anisotropic two-dimensional material borophene. *Nanomaterials* **2021**, *11*, 1165. [CrossRef] [PubMed]
50. Dereshgi, S.A.; Liu, Z.; Aydin, K. Anisotropic localized surface plasmons in borophene. *Opt. Express* **2020**, *28*, 16725–16739. [CrossRef]
51. Wang, Y.; Yu, J.; Mao, Y.F.; Chen, J.; Zhu, J. Stable, high-performance sodium-based plasmonic devices in the near infrared. *Nature* **2020**, *581*, 401–405. [CrossRef] [PubMed]
52. Gao, J.; Hou, C.; Wang, F.; Liu, H.; Ma, T. A directional coupler based on graphene-enhanced Na-loaded plasmonic rib waveguide. *Opt. Commun.* **2021**, *499*, 127316. [CrossRef]
53. Ma, T.; Ma, J.; Liu, H.; Tian, Y.; Liu, S.; Wang, F. Electro-optic tunable directional coupler based on a $LiNbO_3$/Na surface plasmonic waveguide. *Acta Phys. Sin.* **2022**, *71*, 054205. [CrossRef]
54. Rawashdeh, A.; Lupa, S.; Welch, W.; Yang, A. Sodium surface lattice plasmons. *J. Phys. Chem. C* **2021**, *125*, 25148–25154. [CrossRef]

55. Akbar, J.; Bin, X.; Hou, L.; Marsh, J.H.; Liu, X. Surface plasmon polaritons excitation at the interface of graphene and sodium media. *Eur. Phys. J. Plus* **2022**, *137*, 291. [CrossRef]
56. Yang, H.U.; Archangel, J.D.; Sundheimer, M.L.; Tucker, E.; Boreman, G.D.; Raschke, M.B. Optical dielectric function of silver. *Phys. Rev. B* **2015**, *91*, 235137. [CrossRef]
57. Buckley, R.; Berini, P. Figures of merit for 2D surface plasmon waveguides and application to metal stripes. *Opt. Express* **2007**, *15*, 12174–12182. [CrossRef]
58. Teng, D.; Wang, Z.; Huan, Q.; Wang, H.; Wang, K. A low loss platform for subwavelength terahertz graphene plasmon propagation. *Opt. Mater.* **2022**, *128*, 112436. [CrossRef]
59. Said, A.; Atia, K.S.R.; Obayya, S.S.A. On modeling of plasmonic devices: Overview. *J. Opt. Soc. Am. B* **2020**, *37*, A163–A174. [CrossRef]
60. Gerislioglu, B.; Dong, L.; Ahmadivand, A.; Hu, H.; Nordlander, P.; Halas, N.J. Monolithic metal dimer-on-film structure: New plasmonic properties introduced by the underlying metal. *Nano Lett.* **2020**, *20*, 2087–2093. [CrossRef]
61. Gerislioglu, B.; Ahmadivand, A.; Pala, N. Single-and multimode beam propagation through an optothermally controllable Fano clusters-mediated waveguide. *J. Lightwave Technol.* **2017**, *35*, 4961–4966. [CrossRef]
62. Teng, D.; Wang, K.; Huan, Q.; Zhao, Y.; Tang, Y. High-performance transmission of surface plasmons in graphene-covered nanowire pairs with substrate. *Nanomaterials* **2019**, *9*, 1594. [CrossRef] [PubMed]
63. Schinke, C.; Christian Peest, P.; Schmidt, J.; Brendel, R.; Bothe, K.; Vogt, M.R.; Kröger, I.; Winter, S.; Schirmacher, A.; Lim, S.; et al. Uncertainty analysis for the coefficient of band-to-band absorption of crystalline silicon. *AIP Adv.* **2015**, *5*, 067168. [CrossRef]
64. Zhang, X.; Xu, Q.; Xia, L.; Li, Y.; Gu, J.; Tian, Z.; Ouyang, C.; Han, J.; Zhang, W. Terahertz surface plasmonic waves: A review. *Adv. Photon.* **2020**, *2*, 014001. [CrossRef]
65. Knight, M.W.; King, N.S.; Liu, L.F.; Everitt, H.O.; Nordlander, P.; Halas, N.J. Aluminum for plasmonics. *ACS Nano* **2014**, *8*, 834–840. [CrossRef]